Differentiation and Characterization of Rat Mammary Fibroadenomas and 4T1 Mouse Carcinomas Using Quantitative Ultrasound Imaging

Michael L. Oelze*, *Member, IEEE*, William D. O'Brien, Jr, *Fellow, IEEE*, James P. Blue, and James F. Zachary

***Abstract*—Scatterer properties like the average effective scatterer diameter and acoustic concentration were determined *in vivo* using a quantitative ultrasound (QUS) technique from two tumor phenotypes grown in animal models. These tumor models included spontaneously occurring mammary fibroadenomas in rats and transplanted 4T1 mammary carcinomas in mice. The scatterer properties of average scatterer diameter and acoustic concentration were estimated using a Gaussian form factor from the backscattered ultrasound measured from both types of tumors. QUS images of the tumors were constructed utilizing estimated scatterer properties from regions in the tumors. The QUS images showed a clear distinction between the two types of tumors and a statistically significant difference existed between their estimated scatterer properties. The average scatterer diameter and acoustic concentration for the mammary fibroadenomas were estimated to be 105 ± 25 μm and -15.6 ± 5 dB(mm^{-3}), respectively. The average scatterer diameter and acoustic concentration for the carcinomas was estimated to be 28 ± 4.6 μm and 10.6 ± 6.9 dB(mm^{-3}), respectively. The distinctions in the scattering properties are clearly seen in the QUS images of the tumors and indicate that QUS imaging can be useful in differentiating between different types of mammary tumors.**

***Index Terms*—Cancer detection, tissue characterization, ultrasound backscatter, ultrasound imaging.**

I. Introduction

CONVENTIONAL B-mode images of tissues using ultrasound are made by generating a gray-scale image using the envelope-detected radio frequency (RF) signal backscattered from the tissues. The frequency-dependent information contained in the backscattered RF signal is not utilized by conventional B-mode imaging.

The frequency dependence of the backscattered RF signal has been hypothesized to contain information about tissue microstructure [1]–[13]. Ultrasonic backscatter RF spectral information offers the possibility of obtaining microstructure information at spatial scales smaller than can be resolved by conventional B-mode imaging. Estimates of scatterer properties from the RF signal spectrum can be incorporated into enhanced B-mode images called quantitative ultrasound (QUS) images. The QUS images are constructed by converting estimates of scatterer properties to color-coded pixels in an image. The extension in resolvable microstructure has the potential to improve the diagnostic capability of ultrasonic imaging.

QUS images created from scattering property estimates using ultrasound have been used to characterize tissues [2]–[4], [6], [12], [14], [15]. Specifically, QUS imaging based on ultrasound backscatter has been used to extract two tissue properties: average effective scatterer size and acoustic concentration (product of the number concentration of scatterers times the square of the relative impedance difference between the scatterers and surrounding tissue) for the characterization of biological tissues. The effective scatterer size is defined as the -6-dB width of the spatial autocorrelation function (SAF) of acoustic impedance that describes the scatterer [3]. Feleppa *et al.* used frequency-dependent backscatter to quantify the scatterer sizes and acoustic concentration of ocular tumors and the prostate [2], [12]. Lizzi *et al.* used the QUS techniques to examine the structure of the liver [3]. Insana *et al.* used similar techniques to parameterize renal tissue and the ultrasound backscatter was related to structures in the kidney [15]. Numerous other experiments and detailed scattering models have been developed and used to describe backscattered ultrasound from biological tissues [8]. Characterization of tissue and cell organization, cytoarchitectural features, and subcellular organelles (i.e., nuclei and mitotic figures) through QUS imaging techniques (noninvasive) has the potential to develop medically significant approaches to the diagnosis and treatment of disease.

In our previous studies, QUS imaging was used to detect and characterize spontaneous fibroadenomas in rats [16], [17]. Scattering structures in the tumors were qualitatively identified based on a comparison between scatterer property estimates and examination of photomicrographs (i.e., light microscopy) of the same tumors. The present study compares two kinds of mammary tumors using scatterer property estimates and QUS imaging. The first tumor type is a spontaneous rat mammary fibroadenoma. The second type of tumor is a mouse 4T1 mammary carcinoma. Comparison between the microstructure of the two solid tumors was made using QUS imaging and light microscopy.

Manuscript received October 23, 2003; revised February 17, 2004. This work was supported in part by the National Institutes of Health (NIH) under Grant CA09067, Grant CA79179, and Grant F32CA96419 and in part by the University of Illinois Campus Research Board. The Associate Editor responsible for coordinating the review of this paper and recommending its publication was M. Insana. *Asterisk indicates corresponding author.*

*M. L. Oelze is with the Electrical and Computer Engineering Department at the University of Illinois, Urbana, IL 61801 USA (e-mail: oelze@uiuc.edu).

W. D. O'Brien, Jr., is with the Electrical and Computer Engineering Department and the Bioengineering Department at the University of Illinois, Urbana, IL 61801 USA.

J. P. Blue is with the Department of Veterinary Pathobiology at the University of Illinois, Urbana, IL, 61802 USA.

J. F. Zachary is with the Department of Veterinary Pathobiology and the Department and the Bioengineering Department at the University of Illinois, Urbana, IL 61801 USA.

Digital Object Identifier 10.1109/TMI.2004.826953

II. Methods and Procedures

A. Animal Use

The experimental protocol was approved by the campus Laboratory Animal Care Advisory Committee and satisfied all campus and National Institutes of Health rules for the humane use of laboratory animals.

B. Rat Fibroadenomas

Eight Sprague–Dawley mature female rats (Harlan, Indianapolis, IN) that had spontaneous mammary fibroadenomas were evaluated. This tumor was chosen because of its relatively heterogeneous structural characteristics. Tumor epithelial cells were relatively uniform in morphology, arranged in well-defined groups (i.e., acini), and polygonal to elongate in shape with large prominent nuclei. Extracellular matrix was abundant and consisted of broad bands of fibrous connective tissue dispersed between acini. This structural relationship provided sharp differences in tissue characterization from region to region (i.e., heterogeneous scatterer environment).

Before scanning, each rat was euthanized with CO_2, and the tumor and surrounding area were immediately shaved with electric clippers and depilated (Nair, Carter-Wallace, Inc., New York, NY). The rat was then placed in a holder in a tank of degassed water at 37 °C for scanning with an ultrasonic transducer.

A single-element, weakly focused transducer was used to scan laterally across the tumors and surrounding tissues. The transducer had an aperture diameter of 12 mm and a focus at 50 mm. The center frequency of the transducer was 8.5 MHz with a −6-dB pulse/echo frequency bandwidth of 7 MHz measured from the reference spectrum. The power spectrum was measured for particular regions of interest (ROIs) by taking the magnitude squared of the Fourier transform of gated sections from the backscattered time signal. The effects of the equipment on the power spectrum measurement were factored out by dividing by the reference spectrum [5], [6]. To obtain the calibration (reference) spectrum, a pulse was reflected from a planar, Plexiglas surface with known reflectivity and received by the emitting transducer. The same transducer, equipment and settings were used to send and receive the reflected pulses that were used to obtain the backscattered signals from selected ROIs in the tissue. Each ROI was associated with a reference spectrum located at the same axial distance from the source/receiver. The measured power spectrum of the signal from the gated ROI in the tissue was divided by the power spectrum of the reference signal. Estimates of scatterer properties were made within the depth of focus of the transducer from the measured power spectrum. The frequency and bandwidth were chosen based on the expected values of the average scatterer sizes in the rat tissues.

The transducer was operated in pulse/echo mode through a Panametrics 5800 pulser/receiver (Waltham, MA). Echo signals were recorded and digitized on an oscilloscope (Lecroy 9354 TM; Chestnut Ridge, NY) and downloaded to a PC computer for postprocessing. The sampling rate used to digitize the received signals was 200 MHz. The transducer was moved laterally across the chest and tumor by a micropositioning system with step size of a 100 μm between each scan line. The attenuation assumed for the rats was 0.9 dB/cm/MHz and was based on reports of attenuation measurements in the chest walls of rats and mice [18].

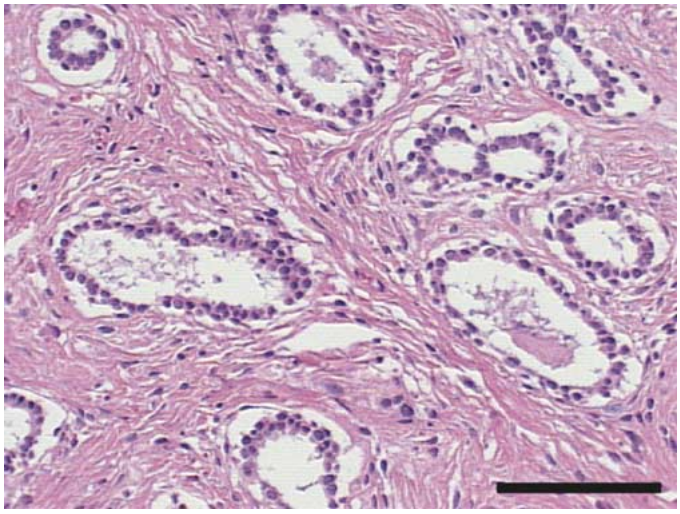

Fig. 1. Photomicrograph of a rat mammary fibroadenoma. The specimen was fixed in 10% neutral buffered formalin, dehydrated, embedded in paraffin, sectioned at 5 μm, mounted on a glass slide, and stained with hematoxylin and eosin for microscopic evaluation. The tumor consists of well-differentiated epithelial cells arranged in acini surrounded by bands of fibrous connective tissue. The scale bar represents 100 μm.

After scanning, tumors were excised, fixed in 10% neutral-buffered formalin, processed and embedded in paraffin, sectioned at 5 μm, and stained with hematoxylin and eosin for routine histologic evaluation by light microscopy. The tumors were diagnosed as mammary fibroadenomas following histopathologic evaluation. Fig. 1 shows the histopathologic characteristics of a mammary fibroadenoma using light microscopy. The tumor consisted of well-differentiated mammary epithelial cells arranged in acini surrounded by broad bands of fibrous connective tissue.

C. Mouse Carcinomas

A mouse mammary tumor cell line (4T1 [CRL-2539]) was purchased from American Type Culture Collection (ATCC, Manassas, VA). This cell line was chosen because of its homogeneous cytologic characteristics. These cells were relatively uniform in morphology, oval to polygonal in shape with large prominent nuclei. Extracellular matrix was minimal to nonapparent. We used these cells as an *in vivo* model for uniform scattering statistics in tissues. This tumor cell line is also a model for stage IV human breast cancer [19]–[21].

4T1 cells were stored at −70 °C, thawed at 37 °C in a water bath, grown in RPMI 1640 medium with 10% fetal bovine serum (FBS) and antibiotic/antifungal supplements (ATCC, Manassas, VA), and incubated at 37 °C at 100% humidity and 5% CO_2. Cells were grown in 75 cm^2 tissue culture flasks (T-75, Corning Incorporated, Corning, NY). When cells were 80% confluent (i.e., adherent cell line), they were rinsed with RPMI 1640 medium lacking FBS or supplements and then covered with 2.0 mL of Trypsin-EDTA (ATCC, Manassas, VA)

to detach the cells from the flask. The cells were gently and repetitively drawn through a 10-mL pipette to individualize the cells. The number of cells present in an 80% confluent flask was determined to be approximately 10^7 cells/mL.

Detached cells were washed two times with 10 mL of RPMI 1640 medium lacking FBS or supplements and resuspended in RPMI 1640 medium lacking FBS or supplements to concentration of 10^5 cells/mL. The abdominal mammary fat pad of anesthetized 8- to 16- week-old female BALB/c mice (Harlan, Indianapolis, IN) was injected with 0.1 mL of suspended 4T1 cells (approximately 10^4 cells). The number of cells injected was shown to initiate tumor growth in 100% of mice within 8–10 days postinjection [19]. Tumors with a diameter of 1.0 cm or greater were used for QUS imaging.

Mice were weighed and anesthetized with ketamine hydrochloride (87.0 mg/kg) and xylazine (13.0 mg/kg) administered intraperitoneally when they were injected with 4T1 cells. After the tumors reached 1.0 cm in diameter, mice were reanesthetized and killed under anesthesia by cervical dislocation. The tumors were then ultrasonically imaged.

A total of 20 mice were used in the study. For each mouse, the tumor and surrounding area were immediately shaved with electric clippers and depilated (Nair). The mouse was then placed on a holder in a tank of degassed water at 37 °C for scanning with an ultrasonic transducer.

Two single-element weakly focused transducers were used to scan 10 mice each. The first transducer had a measured center frequency of 8.5 MHz at the focus with a −6-dB pulse/echo frequency bandwidth of 7 MHz (5–12 MHz) from the reference spectrum. The aperture diameter of this transducer was 12 mm with a focus at 50 mm. Estimates of scatterer properties were made within the depth of focus of the transducer.

Initial scatterer size estimates with the 8.5-MHz transducer were made and found to have a ka value below optimal ($\leq$0.5). Scatterers corresponding to ka values less than 0.5 (30–40 μm for the 8.5-MHz transducer) are difficult to distinguish from point or Rayleigh scatterers [22]. The second transducer was chosen in order to take measurements within a more optimal ka range. This transducer had a measured center frequency of 20 MHz at the focus with a 75% −6-dB pulse/echo bandwidth (10–25 MHz). The aperture diameter of the 20-MHz transducer was 6 mm with a focus measured at 20 mm.

The 8.5-MHz and 20-MHz transducers were operated in pulse/echo mode through Panametrics 5800 and 5900 pulser/receivers, respectively. The signals were recorded and digitized on an oscilloscope (Lecroy 9354 TM) and downloaded to a PC computer for postprocessing. The sampling rate of the received echo signals was 200 MHz. The transducers were moved laterally across the tumor by a micropositioning system with step size between each scan line of a 100 μm for the 8.5-MHz transducer and 50 μm for the 20-MHz transducer. The attenuation assumed for the mouse experiments was 0.4 dB/cm/MHz based on insertion loss measurements from sliced carcinoma tissues. The difference in attenuation between the two kinds of tumors was in itself an important characteristic for differentiation. If frequency-dependent attenuation losses are not compensated, estimates of scatterer size will be larger. In the case of the two tumors, if the same attenuation value were used for both tumors, the differences in the scatterer size would have been greater [23].

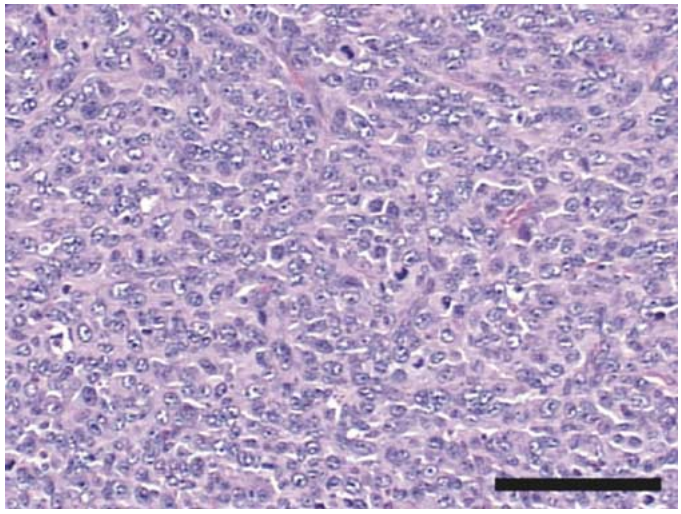

Fig. 2. Photomicrograph of a mouse 4T1 mammary carcinoma. The specimen was fixed in 10% neutral buffered formalin, dehydrated, embedded in paraffin, sectioned at 5 μm, mounted on a glass slide, and stained with hematoxylin and eosin for microscopic evaluation. The tumors consisted of the carcinoma cells with relatively uniform morphology and minimal extracellular matrix. The scale bar represents 100 μm.

After scanning, the tumors were excised, processed, and evaluated as previously described. Fig. 2 shows a photomicrograph of a tissue slice through a tumor using light microscopy. The carcinoma had a relatively uniform morphology (i.e., homogenous scatterer environment) and minimal extracellular matrix. The cells were oval to polygonal in shape with prominent nuclei and a cytoplasmic volume 50%–200% greater than the nuclear volume. The ratio of cytoplasmic volume relative to nuclear volume was made by visually estimating the nuclear volume and total cell size from photomicrographs.

D. Estimation Routines

Acoustic scattering theories for biological tissues assume that the tissues can be modeled as inhomogeneous fluids [10]. Scattering occurs when an acoustic wave interacts with a region that has different impedance relative to the surrounding tissue or fluid. Acoustic signals backscattered from biological tissues contain information about the size, shape, number and relative impedance of the scattering regions within the tissues. Typically, at any instant in time, the backscattered signal will be a superposition of echo signals from numerous small structures confined within the volume of ensonified tissue. The backscattered signal is, therefore, modeled as a statistical distribution of scatterers in size and acoustic concentration.

The scatterer property estimates can be made by comparing the backscattered power spectrum of the RF signal gated from each ROI to a theoretical backscattered power spectrum. The backscattered power spectrum is the magnitude squared of the Fourier transform of the gated RF signal. The theoretical backscattered power spectrum has been modeled from a three-dimensional (3-D) SAF describing the shape and distribution of scatterers in the medium [5], [13], [14], [22]. The SAF models work for soft tissues that do not support

shear waves. Recent modeling of bone with a SAF has shown success in predicting the backscattered power spectrum [24]. If the scattering sites are assumed to be of a particular shape or form and to be randomly distributed (incoherent scattering), then for simple geometric shapes, e.g., spheres or cylinders, closed-form solutions for the SAF can be obtained. These shapes can be represented as fluid filled spheres or cylinders, shells, or even continuous functions of changing impedance, i.e., the Gaussian scatterer. From the closed-form solutions of the SAF, closed-form solutions for the theoretical backscattered power spectrum can be calculated. The theoretical backscattered power spectrum is given by

$$W_{theor}(f) = B(L,q)C(a_{eff}, n_z)f^4F(f, a_{eff}) \qquad (1)$$

where f is the frequency (megahertz), C is a constant depending on the average effective radius, a_{eff}, of the scatterers (mm) and the average acoustic concentration, n_z, of scatterers (mm^{-3}), B is a constant depending on the length of the gate, L, and the ratio of the aperture radius to distance from the region of interest, q, and F is called the form factor and is a function of the frequency and average effective scatterer radius [5], [6].

The form factor (FF) describes frequency dependence of scattering based on the size, shape, and mechanical properties of the scatterers. An important consideration for accurately estimating scatterer properties is the appropriate choice of the FF. The Gaussian FF has been used to model the scattering properties of many soft tissues [1], [3]–[5], [10], [13]. The Gaussian FF represents a distribution of continuously changing impedance with the surrounding tissues unlike a rigid or fluid filled sphere that would represent an abrupt change with the surrounding soft tissue. Furthermore, the Gaussian scatterer would have an effective radius related to the impedance distribution of the scatterer, unlike the definite radius describing a spherical shell or fluid filled sphere. The Gaussian FF is given by [17]

$$F_{\mathrm{gauss}}(f) = e^{-12.3f^2a_{eff}^2}. \qquad (2)$$

The constant in (2) normalizes the FF, assuming a speed of sound in the tissue of interrogation of 1540 m/s, so that the effective scatterer radius represents the width of the -6-dB edge of the Gaussian function [3]. The theoretical power spectrum was defined by inserting (2) into (1). Gating and lateral beam pattern effects were incorporated into the theoretical power spectrum according to Lizzi *et al.* for the spherical Gaussian scatterer yielding [13]

$$W_{theor}(f) = \frac{185Lq^2a_{eff}^6n_zf^4}{[1+2.66(fqa_{eff})^2]}e^{-12.3f^2a_{eff}^2}. \qquad (3)$$

The measured backscattered power spectrum for an ROI was found by averaging the backscattered power spectra measured from the echo signals corresponding spatially to the ROI. The measured backscattered power spectrum is given by [6]

$$W_{\mathrm{comp}}(f) = \frac{1}{N}A(f,L)\sum_{n=1}^{N}\frac{|FT\{p_n(t)\}|^2}{W_{\mathrm{ref}}(f)} \qquad (4)$$

where $FT\{p_n(t)\}$ represents the Fourier transform of the gated RF signal of the nth scan line, N is the number of gated scan lines, $A(f,L)$ is a frequency-dependent attenuation-compensation function [23] and $W_{\mathrm{ref}}(f)$ is the reference power spectrum. The effects of the equipment on the power spectrum measurement were factored out by dividing by a reference spectrum [5], [6], [25]. The measured backscattered power spectrum was compensated for attenuation losses according to the frequency-dependent attenuation-compensation function, $A(f,L)$, derived for echo signals gated with Hanning windows [23].

Estimates of the scatterer properties were made using the technique of Oelze *et al.* [16] by comparing the logarithm of the measured backscattered power spectrum, (4), with the logarithm of the theoretical power spectrum, (3)

$$10\log_{10}W_{\mathrm{comp}}(f) \approx 10\log_{10}f^4 + m(a_{eff},q)f^2 + b(n_z, a_{eff}, L, q). \qquad (5)$$

Subtracting $10\log_{10}f^4$ from both sides of (5) and letting $x = f^2$ yields

$$10\log_{10}W_{\mathrm{comp}}(x) - 10\log_{10}x^2 \approx m(a_{eff},q)x + b(n_z, a_{eff}, q, L). \qquad (6)$$

Equation (6) describes a straight line where the slope, m, is a function of a_{eff} and q, and the intercept, b, is a function of a_{eff}, n_z, q, and L. The quantity q is determined by the characteristics of the operating transducer and L is known. To obtain the scatterer estimates, least-squares analysis was used to find the best-fit slope and intercept to the linearized, log average backscattered power spectrum of (6) [16], [17]. Once the average effective scatterer radius was estimated from the slope of (6), the acoustic concentration was estimated from the intercept and estimate of the average scatterer diameter. Typically, acoustic concentration values span a large dynamic range. Therefore, estimates of acoustic concentration were expressed in a decibel scale

$$n_{z_{\mathrm{dB}}} = 10\log n_z \qquad (7)$$

referenced to an acoustic concentration, n_z, equal to unity.

E. Construction of QUS Images

B-mode images were constructed for each rat and mouse experiment. From the B-mode images, ROIs were selected inside the tumors where the B-mode images appeared to be homogeneous (no interfaces or large echoes). The RF echoes were gated lines within each ROI using a sliding Hanning window with a 66% overlap. Each ROI was a square 3 mm $\times$ 3 mm for the 8.5-MHz data and 1.5 mm $\times$ 1.5 mm for the 20-MHz data. The side lengths of the ROIs were chosen so that length of the gated signal would be around 20 wavelengths of the center frequency. Topp *et al.* showed that estimated spectrum parameters were independent of gate length (after normalizing for the length of the gate, L) when the length of the gated signal was at least 10 wavelengths of the center frequency in the analysis bandwidth [26]. The longer the gated length the more accurate and precise the estimate. The lateral length of an ROI was chosen to be 5 beamwidths in size.

Scatterer property estimates were made for each ROI using the best-fit line estimation scheme for the Gaussian form factor

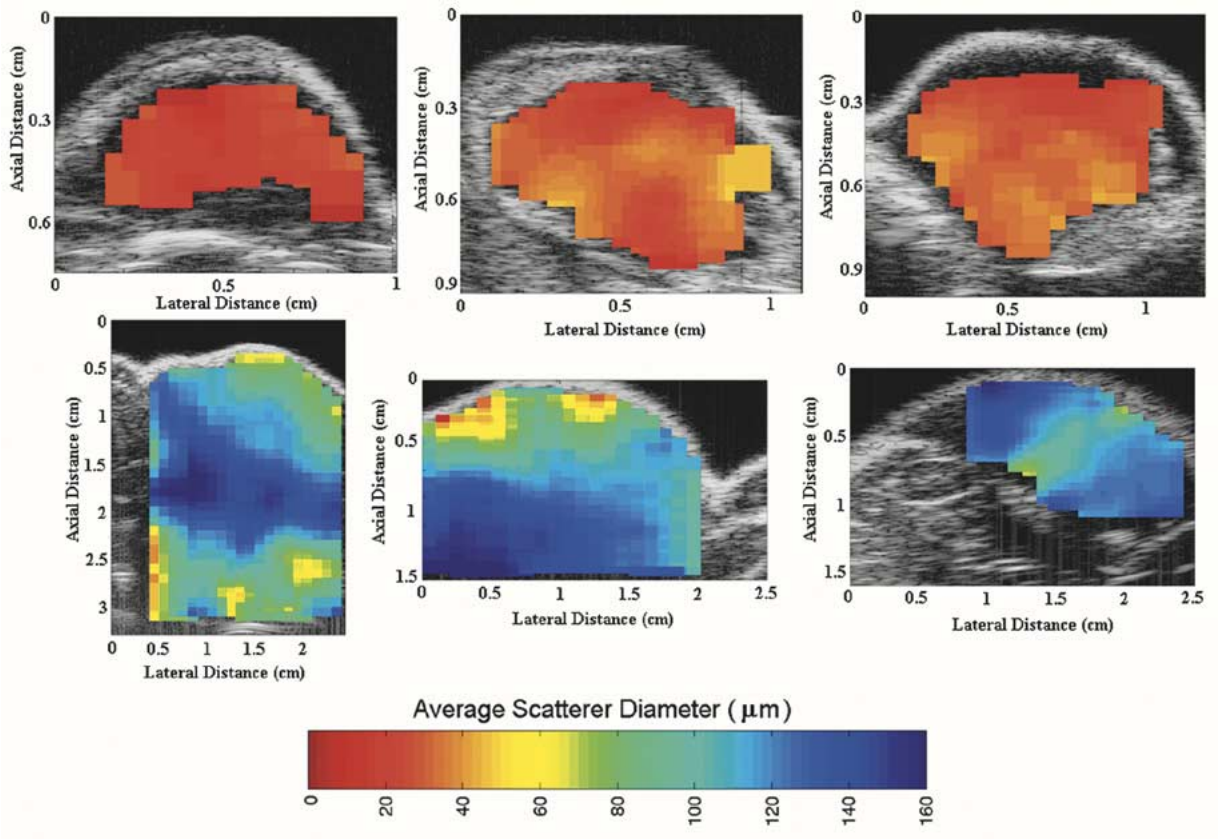

Fig. 3. QUS images of mouse carcinomas (top panel) made at 20 MHz and rat fibroadenomas (middle panel) using the estimated average scatterer size. The colorbar (bottom panel) shows the relation between the color encoding and the average scatterer sizes.

model, (6) [16], [17]. Each ROI was overlapped by another ROI both laterally and axially by 66%. Pixels of 1 mm × 1 mm and 0.5 mm × 0.5 mm in size for the 8.5-MHz and 20-MHz data were defined, respectively. Each pixel was associated with scatterer property estimates averaged from corresponding, overlapping ROIs. The color of each pixel was assigned based on the value of the averaged, scatterer property estimate associated with the pixel. The colored pixels were then superimposed on the gray-scale B-mode images of the rats and mice to create QUS images. Color bars, displayed with the QUS images, show the relationship between the colored pixels and the scatterer property estimates.

III. Experimental Results

QUS images were constructed from scans of the spontaneous fibroadenomas and the 4T1 mammary carcinomas, and then were compared. Fig. 3 shows several gray-scale, B-mode images with color overlays that depict the average scatterer size. The color bar relates the pixels in the QUS images to the estimated scatterer sizes in the particular ROIs. A clear distinction between the carcinomas and the fibroadenomas is apparent in the scatterer-size, QUS images. The QUS images indicate that the carcinomas have smaller, more-homogeneous scatterers than the fibroadenomas. The carcinomas are characterized by red and orange pixels that indicate smaller scatterer sizes while the fibroadenomas are characterized predominantly by blue pixels but also present a wide range of pixel color. Fig. 4 shows several gray-scale, B-mode images with color overlays that depict average acoustic concentration. A clear distinction is apparent between the mouse carcinomas and the rat fibroadenomas in these acoustic-concentration images. These QUS images indicate that the carcinomas have larger acoustic concentrations than the fibroadenomas. The higher values of acoustic concentration are shown by the blue to green colored pixels for the carcinomas while the smaller values are shown by the colors dominated by orange and yellows pixels for the fibroadenomas.

After each QUS image was constructed, the mean values of scatterer property estimates inside the tumor were calculated. Fig. 5 is a bar graph showing the overall average estimated scatterer diameters in the rat fibroadenomas and in the mouse carcinomas. Similarly, Fig. 6 is a bar graph of the estimated overall average acoustic-concentration values in the rat fibroadenomas and in the mouse carcinomas. The average scatterer diameter and acoustic concentration for the fibroadenomas were estimated at 105 ± 14 μm and -15.6 ± 5 dB(mm^{-3}), respectively. The average scatterer diameter and acoustic concentration for the carcinomas (20 MHz) were estimated to be 28 ± 4.6 μm and 10.6 ± 6.9 dB(mm^{-3}), respectively. For the 8.5-MHz carcinoma data, the average scatterer diameter and acoustic concentration were estimated to be 39.8 ± 6.4 μm and 21.3 ± 5.9 dB(mm^{-3}), respectively.

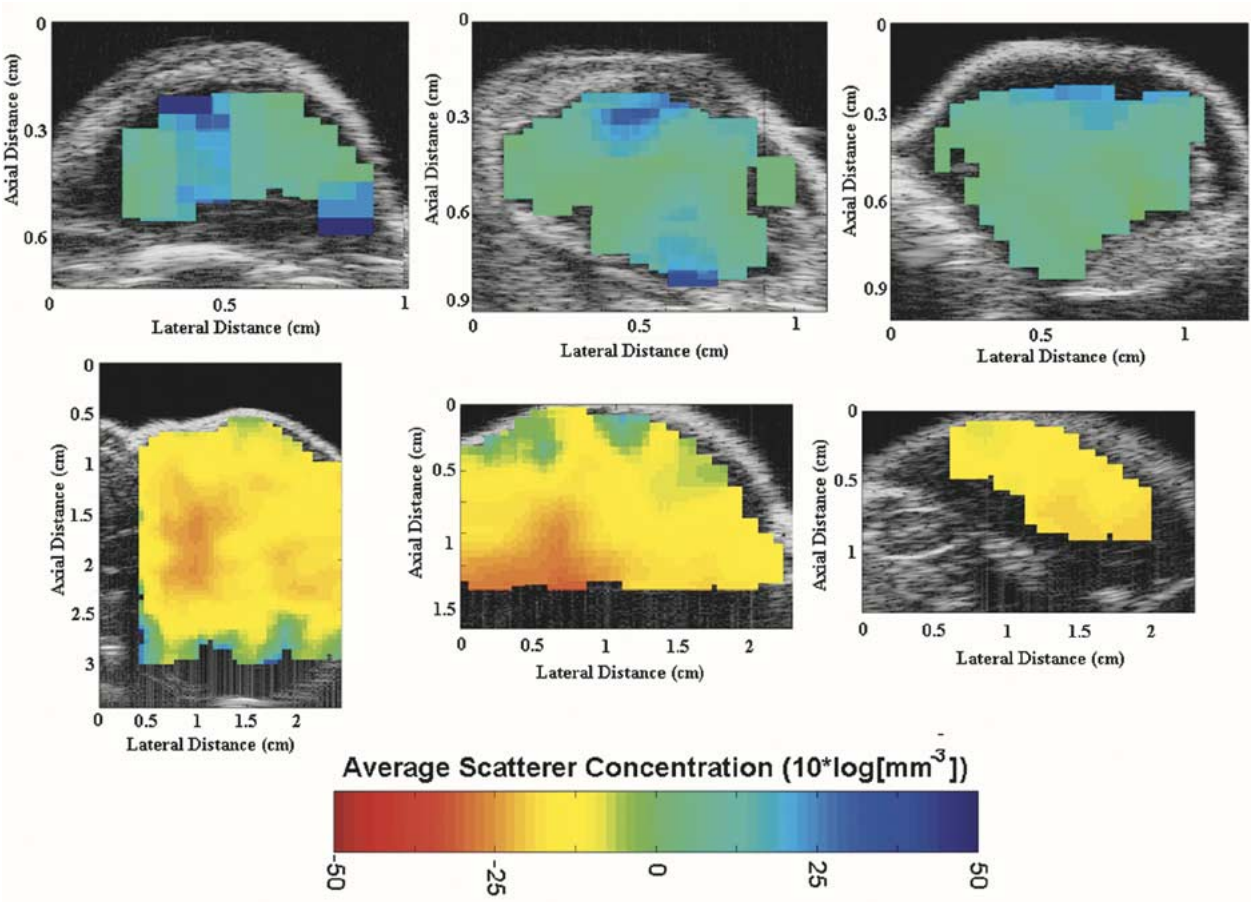

Fig. 4. QUS images of mouse carcinomas (top panel) made at 20 MHz and rat fibroadenomas (middle panel) using the estimated average acoustic concentration. The colorbar (bottom panel) shows the relation between the color encoding and the average acoustic concentration.

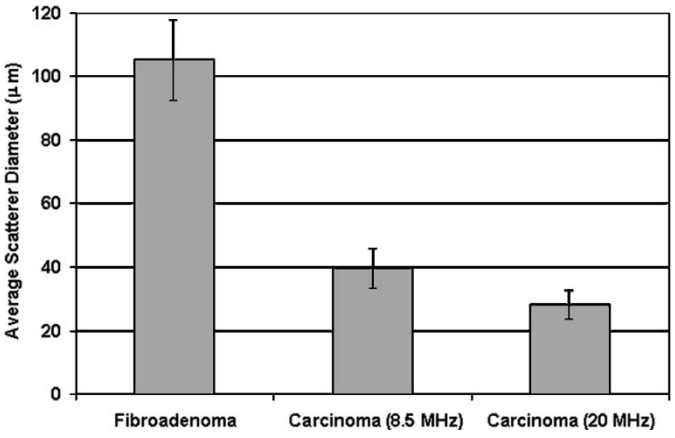

Fig. 5. Bar graph of the average scatterer diameter values for the rat fibroadenomas and the mouse carcinomas.

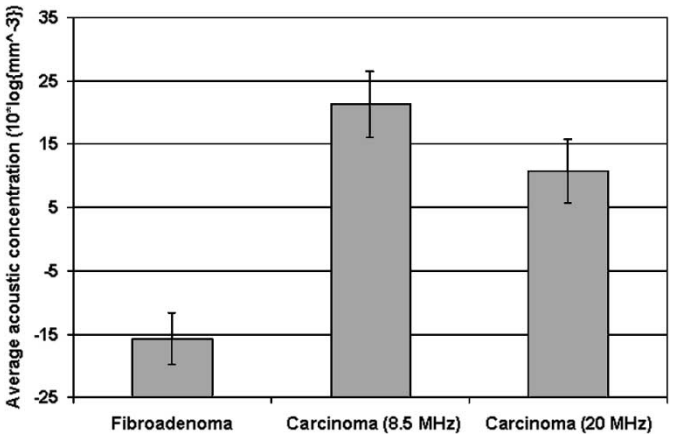

Fig. 6. Bar graph of the average acoustic concentration values for the rat fibroadenomas and the mouse carcinomas.

The differences in the estimates from the two transducers indicated that the technique was sensitive to the ka range used in the measurements. The differences in the estimates may be due to several things. First, using a smaller ka range leads to less accurate estimates because a smaller portion of the spectrum will be mapped out. Further, the Gaussian FF tends to be more flat at the lower ka values [5] making distinguishing between different scatterer sizes more difficult. Second, if the frequency-dependent attenuation values were overestimated, the estimates made using the higher frequencies would tend to underestimate the size more than the lower frequency estimates [23]. Finally, the Gaussian FF was used to model both kinds of tumors. However, improved FFs may be constructed in the future that better fit the measured data and reflect the underlying structure. Building better models will lead to more accurate estimates of scatterer properties over a broader range of ka values.

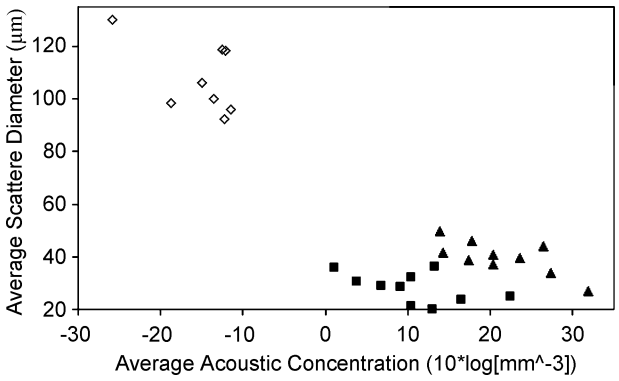

Fig. 7. Feature analysis plot of the average scatterer acoustic concentration versus the average scatterer diameter for estimates made; ◇,inside the fibroadenoma; ▲, inside the carcinoma (8.5 MHz); ■, inside the carcinoma (20 MHz).

Statistically significant differences existed between QUS parameter values of the mouse carcinomas and rat fibroadenomas. Analysis of the variance resulted in a p-value <0.05 between scatterer-size and acoustic-concentration estimates for these two tumor types. Likewise, a statistically significant difference between scatterer acoustic concentration estimates from the rat fibroadenomas and mouse carcinomas was observed. The combined average from each rat revealed the estimated scatterer diameters inside the fibroadenomas were 3.8 times larger than estimates from inside the carcinoma tumors at 20 MHz (2.7 times for the 10 mouse scatterer size estimates made at 8.5 MHz). Scatterer sizes for all mouse carcinomas were in each case found to be much smaller than estimates made in the fibroadenomas (Fig. 5). Similarly, the average acoustic concentration was much smaller for the rat fibroadenomas than for the mouse carcinomas.

Fig. 7 is a feature analysis plot with the estimated acoustic scatterer concentration versus the estimated scatterer sizes for the 8 rats and the 20 mice. The 20-MHz estimates should be superior to the 8.5-MHz estimates because the ka range is optimal for making estimates than from the 8.5-MHz transducer (ka range from 0.6 to 1.4 for 20 MHz as opposed to 0.3 to 0.7 for 8.5 MHz). The 20-MHz data gave smaller and more consistent scatterer size estimates, indicating the importance of optimizing the ka range.

A clear distinction is seen between the different tumor types. Qualitative comparisons between photomicrographs of the fibroadenomas and carcinomas identified prominent structures similar in size to the QUS estimates. Glandular acini in the fibroadenoma appeared to have an average size of around 100 μm [17]. Qualitatively, the carcinoma exhibited an average cell nuclear diameter of around 13.8 μm with total cell sizes ranging from 50% to possibly 200% larger than the nucleus.

The average nuclear size in the carcinoma was estimated by converting a photomicrograph of a carcinoma into a bitmap. The photomicrograph represents a two-dimensional (2-D) slice of a 3-D volume. Assuming the nuclei were spherical, the nuclei were represented by a circle in the 2-D photomicrograph. The area of each nucleus in the photomicrograph was a function of the actual size of the nucleus, the thickness of the slice (3 μm) and the point of the nucleus where the slice was made. If the slice were made across the middle of the nucleus, then the area would appear maximized. If the slice were made across the bottom of the nucleus, the area would appear much smaller. The actual diameter of a nucleus could be calculated from a nucleus that was sliced across its middle. The nuclei in the bitmap image were outlined and filled in with the color white while all else was filled in with the color black. The ten largest nuclei were selected from the bitmap image and the areas of the ten largest nuclei were estimated by counting the number of pixels corresponding to the nuclei. Fig. 8 is a bitmap image representing the ten largest nuclei. The ten largest nuclei were chosen because they were hypothesized to represent the nuclei that were sectioned across their middle as opposed to their edge. The areas of the 10 nuclei were then used to calculate an average diameter of the nuclei. The average diameter, 13.8 μm, was used as the estimate of the average nuclear size for all carcinoma cells.

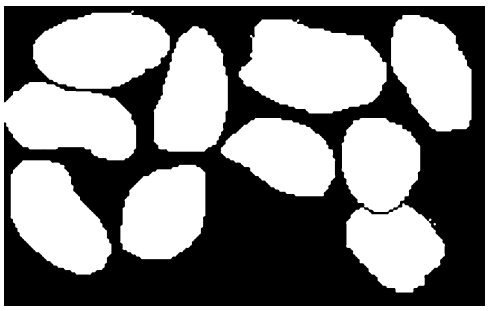

Fig. 8. Bitmap image of the ten largest nuclei chosen from a photomicrograph section of a carcinoma tumor. The nuclei are colored white. Each pixel represents 3.1 μm^2.

IV. Conclusion

In this study, eight rats with spontaneous mammary fibroadenomas and 20 mice with 4T1 transplanted mammary carcinomas were examined using QUS imaging. Estimates of properties of the tissue microstructure were made from the frequency dependence of the ultrasound backscatter. QUS images were constructed that superimposed color-coded pixels related to the estimates of average scatterer properties; scatterer diameter and acoustic concentration. The study revealed that QUS imaging based on estimated scatterer properties was able to distinguish between mammary fibroadenomas in rats and carcinomas in mice.

By estimating physical scatterer properties, a limited comparison between QUS images and light microscopic images was made. The qualitative comparison indicated that the QUS imaging technique was able to track different structure sizes for the different kinds of solid tumors. Furthermore, qualitative estimates of the size of cellular structures from the light microscopic images showed similar size estimates to ultrasound. While there will not be an exact one-to-one correlation between optical techniques and acoustic properties and responses, the similarity of size estimates suggest that optical method can help validate ultrasound measurements and theory.

A clear distinction was seen between the fibroadenomas and the carcinomas based on the scatterer property estimates. A statistical difference was seen between the fibroadenomas and the carcinomas for scatterer size and acoustic concentration

estimates. The average scatterer size estimates were larger in the fibroadenomas than in the carcinomas. The average acoustic-concentration value was higher for the carcinomas than for the fibroadenomas. The QUS images also showed the other distinctive features of the two kinds of tumors. The scatterer-size QUS images showed the carcinomas to have smaller, more uniform scatterer sizes (orange to red pixels) while they showed the fibroadenomas to have larger, less uniform scatterer sizes (dominated by deep blue pixels but ranging across the color spectrum). Furthermore, acoustic concentration QUS images showed the carcinomas to have larger acoustic concentrations (blue and green pixels) while they showed the fibroadenomas to have smaller acoustic concentrations of scatterers (yellow to orange pixels). The differences suggest that estimates of the scatterer properties may be useful in discerning between different tissue types and that QUS imaging using scatterer-property estimates may be an important diagnostic tool.

QUS imaging has been shown to be capable of differentiating between scatterer properties in two kinds of solid tumors in rats and mice. The study of QUS imaging of tumors through quantification of real physical properties of the microstructure is an important means of noninvasively diagnosing and monitoring disease. Future studies in our laboratories will focus on determining the anatomical structures responsible for scattering within the tumors and on exploring optical means to help verify ultrasound measurements and theory.

ACKNOWLEDGMENT

The authors would like to thank R. J. Miller, DVM, for her technical assistance.

REFERENCES

[1] D. Nicholas, "Evaluation of backscattering coefficients for excised human tissues: results, interpretation and associated measurements," *Ultrasound Med. Biol.*, vol. 8, pp. 17–28, 1982.

[2] E. J. Feleppa, F. L. Lizzi, D. J. Coleman, and M. M. Yaremko, "Diagnostic spectrum analysis in ophthalmology: a physical perspective," *Ultrasound Med. Biol.*, vol. 12, pp. 623–631, 1986.

[3] F. L. Lizzi, M. Ostromogilsky, E. J. Feleppa, M. C. Rorke, and M. M. Yaremko, "Relationship of ultrasonic spectral parameters to features of tissue microstructure," *IEEE Trans. Ultrason. Ferroelect. Freq. Contr.*, vol. UFFC-33, pp. 319–329, 1986.

[4] D. K. Nassiri and C. R. Hill, "The use of angular scattering measurements to estimate structural parameters of human and animal tissues," *J. Acoust. Soc. Amer.*, vol. 87, pp. 179–192, 1990.

[5] M. F. Insana, R. F. Wagner, D. G. Brown, and T. J. Hall, "Describing small-scale structure in random media using pulse-echo ultrasound," *J. Acoust. Soc. Amer.*, vol. 87, pp. 179–192, 1990.

[6] M. F. Insana and T. J. Hall, "Parametric ultrasound imaging from backscatter coefficient measurements: image formation and interpretation," *Ultrason Imag.*, vol. 12, pp. 245–267, 1990.

[7] M. F. Insana, J. G. Wood, and T. J. Hall, "Identifying acoustic scattering sources in normal renal parenchyma from the anisotropy in acoustic properties," *Ultrasound Med. Biol.*, vol. 18, pp. 587–599, 1992.

[8] K. K. Shung and G. A. Thieme, *Ultrasonic Scattering in Biological Tissues*. Boca Raton, FL: CRC Press, 1993.

[9] M. F. Insana, T. J. Hall, J. G. Wood, and Z.-Y. Yan, "Renal ultrasound using parametric imaging techniques to detect changes in microstructure and function," *Invest. Radiol.*, vol. 28, pp. 720–725, 1993.

[10] M. F. Insana, "Modeling acoustic backscatter from kidney microstructure using an anisotropic correlation function," *J. Acoust. Soc. Amer.*, vol. 97, pp. 649–655, 1995.

[11] T. J. Hall, M. F. Insana, L. A. Harrison, and G. G. Cox, "Ultrasonic measurement of glomerular diameters in normal adult humans," *Ultrasound Med. Biol.*, vol. 22, pp. 987–997, 1996.

[12] E. J. Feleppa, T. Liu, A. Kalisz, M. C. Shao, N. Fleshner, and V. Reuter, "Ultrasonic spectral-parameter imaging of the prostate," *Int. J. Imag. Syst. Technol.*, vol. 8, pp. 11–25, 1997.

[13] F. L. Lizzi, M. Astor, T. Liu, C. Deng, D. J. Coleman, and R. H. Silverman, "Ultrasonic spectrum analysis for tissue assays and therapy evaluation," *Int. J. Imag. Syst. Technol.*, vol. 8, pp. 3–10, 1997.

[14] J. A. Zagzebski, Z. F. Lu, and L. X. Xao, "Quantitative ultrasound imaging: *In vivo* results in normal liver," *Ultrason. Imag.*, vol. 15, pp. 335–351, 1993.

[15] M. F. Insana, J. G. Wood, and T. J. Hall, "Identifying acoustic scattering sources in normal renal parenchyma *in vivo* by varying arterial and ureteral pressures," *Ultrasound Med. Biol.*, vol. 17, pp. 613–626, 1991.

[16] M. L. Oelze, J. F. Zachary, and W. D. O'Brien Jr., "Characterization of tissue microstructure using ultrasonic backscatter: theory and technique for optimization using a Gaussian form factor," *J. Acoust. Soc. Amer.*, vol. 112, pp. 1202–1211, 2002.

[17] ——, "Parametric imaging of rat mammary tumors *in vivo* for the purposes of tissue characterization," *J. Ultrasound Med.*, vol. 21, pp. 1201–1210, 2002.

[18] G. A. Teotica, R. J. Miller, L. A. Frizzell, J. F. Zachary, and W. D. O'Brien Jr., "Attenuation coefficient estimates of mouse and rat chest wall," *IEEE Trans. Ultrason., Ferroelect., Freq. Contr.*, vol. 48, pp. 593–600, Mar. 2001.

[19] B. A. Pulaski and S. Ostrand-Rosneberg, "Reduction of established spontaneous mammary carcinoma metastases following immunotherapy with major histocompatibility complex class II and B7.1 cell-based tumor vaccines," *Cancer Res.*, vol. 58, pp. 1486–1493, 1998.

[20] B. A. Pulaski, D. S. Terman, S. Kahn, E. Muller, and S. Ostrand-Rosneberg, "Cooperativity of staphylococcal aureus enterotoxin B superantigen, major histocompatibility complex class H, and CD80 for immunotherapy of advanced spontaneous metastases in a clinically relevant postoperative mouse breast cancer model," *Cancer Res.*, vol. 60, pp. 2710–2715, 2000.

[21] C. J. Aslakson and F. R. Miller, "Selective events in the metastatic process defined by analysis of the sequential dissemination of subpopulations of a mouse mammary tumor," *Cancer Res.*, vol. 52, pp. 1399–1405, 1992.

[22] T. Hosokawa, B. Sigel, J. Machi, H. Kitamura, R. V. Kolecki, J. R. Justin, E. J. Feleppa, G. Tuszynski, and T. Kakegawa, "Experimental assessment of spectrum analysis of ultrasonic echoes as a method for estimating scatterer properties," *Ultrasound in Med. Biol.*, vol. 20, pp. 463–470, 1994.

[23] M. L. Oelze and W. D. O'Brien Jr., "Frequency-dependent attenuation-compensation functions for ultrasonic signals backscattered from random media," *J. Acoust. Soc. Amer.*, vol. 111, pp. 2308–2319, 2002.

[24] F. Padilla, F. Peyrin, and P. Laugier, "Prediction of backscatter coefficient in trabecular bones using a numerical model of three-dimensional microstructure," *J. Acoust. Soc. Amer.*, vol. 113, pp. 1122–1129, 2003.

[25] F. L. Lizzi, M. Greenbaum, E. J. Feleppa, and M. Elbaum, "Theoretical framework for spectrum analysis in ultrasonic characterization," *J. Acoust. Soc. Amer.*, vol. 73, pp. 1366–1373, 1983.

[26] K. A. Topp, J. F. Zachary, and W. D. O'Brien Jr., "Quantifying B-mode images of *in vivo* rat mammary tumor with frequency dependence of backscatter," *J. Ultrasound Med.*, vol. 20, pp. 605–612, 2001.